

# An extended multi-zone model for the MCG–6-30-15 warm absorber

R. Morales<sup>1</sup>, A.C. Fabian<sup>1</sup> and C.S. Reynolds<sup>2</sup>

1. Institute of Astronomy, Madingley Road, Cambridge CB3 0HA

2. JILA, University of Colorado, Campus Box 440, Boulder, CO 80309-0440 USA

October 26, 2018

## ABSTRACT

The variable warm absorber seen with *ASCA* in the X-ray spectrum of MCG–6-30-15 shows complex time behaviour in which the optical depth of OVIII anticorrelates with the flux whereas that of OVII is unchanging. The explanation in terms of a two zone absorber has since been challenged by *BeppoSAX* observations. These present a more complicated behaviour for the OVIII edge. We demonstrate here that the presence of a third, intermediate, zone can explain all the observations. In practice, warm absorbers are likely to be extended, multi-zone regions of which only part causes directly observable absorption edges at any given time.

**Key words:** galaxies: active – galaxies: individual: MCG–6-30-15 – galaxies: Seyfert – X-rays: galaxies.

## 1 INTRODUCTION

X-ray absorption by partially ionized, optically thin material, along the line of sight of the central engine, the so called *warm absorber*, is one of the prominent features in the X-ray spectrum of many AGN (Reynolds1997). The presence of such gas was first postulated in order to explain the unusual form of the X-ray spectrum of QSO MR 2251-178 (Halpern1984). A direct confirmation of the existence of circumnuclear ionized matter came from *ASCA*, which for the first time was able to resolve the OVII and OVIII absorption edges (at rest energies of 0.74 and 0.87 keV, respectively) in the X-ray spectra of the Seyfert 1 galaxy MCG–6-30-15 (Fabian et al.1994). Systematic studies of warm absorbers in Seyfert 1 galaxies with *ASCA* have shown their ubiquity, being detected in half of the sources (Reynolds1997).

Warm absorbers were usually described by single zone, photoionization equilibrium models. Under this assumption, simple variability patterns were expected: increasing ionization of the matter when the source brightens. This was not found by Otani et al. (1996) during their long-look *ASCA* observation of the nearby ( $z=0.008$ ) Seyfert 1 galaxy MCG–6-30-15. The source varied with large amplitude on short time scales ( $10^4$  s or so). The depth of the OVII edge, on the contrary, stayed almost constant, while that of the OVIII edge was anticorrelated with the flux. To explain the behaviour of the OVII and OVIII edges, the authors adopted a multizone model in which the OVII and OVIII edges originate from spatially distinct regions. OVII ions in the region responsible for the OVII edge, the outer absorber, have a long recombination timescale (i.e. weeks or more), whereas

the OVIII edge arises from more highly ionized material, the inner absorber, in which most oxygen is fully stripped. The recombination timescale for the OIX ions in the inner absorber is of the order of  $10^4$  s or less. A decrease in the primary ionizing flux is then accompanied by the recombination of OIX to OVIII, giving the observed variation in the OVIII edge depth.

Orr et al. (1997) raised the possibility of a more complex warm absorber. During their MCG–6-30-15 *BeppoSAX* observation the depth of the OVII edge was marginally consistent with being constant, whereas the optical depth for OVIII,  $\tau(OVIII)$ , exhibited significant variability. The authors claimed that its large value during epoch 1<sup>\*</sup> ( $1.7 \pm 0.5$ ,  $1\sigma$  uncertainty) was inconsistent with the values at all other epochs. They also pointed out that the value of  $\tau(OVIII)$  during epoch 5 (a low luminosity state) did not show the expected anticorrelation with the ionizing flux.

In both Otani et al. (1996) and Orr et al.(1997),  $\tau(OVIII)$  was plotted versus count rate. In order to compare *ASCA* and *BeppoSAX* observations, these two observational results for  $\tau(OVIII)$  have been plotted versus luminosity<sup>†</sup> in 0.1-10 keV in figure 1 (instead of versus count rate). The conversion from count rate to luminosity is dif-

\* The epochs in the *BeppoSAX* observation are chronologically numerated (i.e. number 1 corresponds to the first epoch of the observation, etc.).

† The conversion from count rate to luminosity has been obtained using  $H_o = 50 \text{ km s}^{-1} \text{ Mpc}^{-1}$ ,  $q_0 = 0$  and PIMMS (<http://heasarc.gsfc.nasa.gov/Tools/w3pimms.html>).

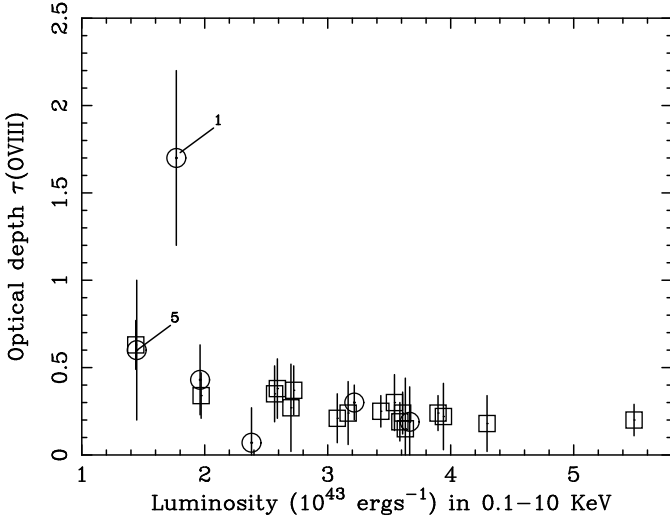


**Figure 1.** Comparison *ASCA* (square) - *BeppoSAX* (circle) observational results for the optical depth of OVIII,  $\tau(OVIII)$ , versus luminosity in 0.1-10 keV. Note the only discrepant point in the *BeppoSAX* observation labelled as 1 and the very good agreement for point 5.

ferent for each apparatus and therefore, the comparison can not be made using count rate, but luminosity. The only discrepancy between both sets of data is the result for epoch 1 (labelled 1 in figure 1)<sup>‡</sup>. Note also that there is no disagreement at all with any other point (Orr et al. mentioned epoch 5 as problematic, but in this plot it appears consistent with the rest of the Otani et al. data).

In this paper we present a simple photoionization model that accounts for the experimental results of both *ASCA* and *BeppoSAX* observations. Section 2 describes the code used to model the inner warm absorber. The application to the MCG-6-30-15 warm absorber is presented in Section 3. The extension of the multi-zone model for the warm absorber (i. e. the third component) is addressed in Section 4. Finally our conclusions are discussed in Section 5.

## 2 TIME DEPENDENT PHOTOIONIZATION CODE

In order to reproduce both *ASCA* and *BeppoSAX* observations, the state of the inner absorber has been modelled using a time dependent photoionization code for oxygen (Reynolds1996). This code treats the material in the inner absorber as containing only ions of oxygen in an otherwise completely ionized hydrogen plasma. A given oxygen ion is assumed to be in one of the 9 states corresponding to its ionization level. Different excitation levels of a given ionization state are not treated. The total abundance of oxygen is fixed at  $7.41 \times 10^{-4}$  (Grevesse1989) relative to hydrogen.

<sup>‡</sup> This epoch was at the very beginning of the *BeppoSAX* observation. In a private communication, A. Orr notes that this high value for the optical depth for OVIII could not be due to instrumental effects, since no similar behaviour, neither at the beginning nor during the observation has been observed in any other *BeppoSAX* target yet.

Both ions and electrons are assumed to be in local thermal equilibrium (LTE) with a common temperature  $T$  and the plasma is assumed to be strictly optically-thin at all frequencies (i.e. radiative transfer processes are not considered).

A point source of ionizing radiation is placed at a distance  $R$  from this material with a frequency dependent luminosity  $L_\nu$  (total luminosity  $L$ ). In the calculations presented here, the ionizing continuum is taken to be a power-law with a photon index  $\Gamma = 2$  extending from  $\nu_{min}$  to  $\nu_{max}$ : i.e. we take

$$L_\nu = \frac{L}{\Lambda\nu} \quad (1)$$

where  $\Lambda = \ln(\nu_{max}/\nu_{min})$ . The upper and lower cutoff frequencies are chosen such that  $h\nu_{max} = 100$  keV, and  $\Lambda = 10$ , corresponding to  $h\nu_{min} \approx 4.5$  eV.

The physical processes included in the code are: photoionization, Auger ionization, collisional ionization, radiative recombination, dielectronic recombination, bremsstrahlung, Compton scattering and collisionally-excited O $\lambda$ 1035 resonance line cooling. Given these processes, the ionization and thermal structure of the plasma is evolved from an initial state assumed to have a temperature of  $T = 10^5$  K, and equal ionization fractions in each state.

The ionization structure of the oxygen is governed by 9 equations of the form:

$$\frac{dn_i}{dt} = \sum_{prod.} \delta_{prod.} - \sum_{dest.} \delta_{dest.} \quad (2)$$

where  $n_i$  is the number density of state- $i$ ,  $\delta$  stands for the ionization/recombination rate per unit volume, the first summation on the right hand side (RHS) is over all ionization and recombination mechanisms that produce state- $i$  and the second summation is over all such mechanisms that destroy state- $i$ .

The thermal evolution of the plasma is determined by the local heating/cooling rate and the macroscopic constraint. The net heating rate per unit volume is given by:

$$\frac{dQ}{dt} = \sum_{heat} \Delta_{heat} - \sum_{cool} \Delta_{cool} \quad (3)$$

where  $\Delta$  stands for the heating/cooling rate per unit volume, the first summation on the RHS is over all heating processes and the second term is over all cooling processes. For a *constant density* plasma, we have  $du = dQ$  where  $u$  is the internal energy per unit volume and is given by:

$$u = \frac{3}{2} n_e k_B T. \quad (4)$$

Thus, the rate of change of temperature is related to the heating/cooling rate via:

$$\frac{dT}{dt} = \frac{2}{3n_e k_B} \frac{dQ}{dt}. \quad (5)$$

The state of the plasma is evolved using the ionization equations represented by (2) and the energy equation (3). A simple step-by-step integration of these differential equation is performed. The time step for the integration process is allowed to dynamically change and is set to be  $0.1 \times t_{sh}$

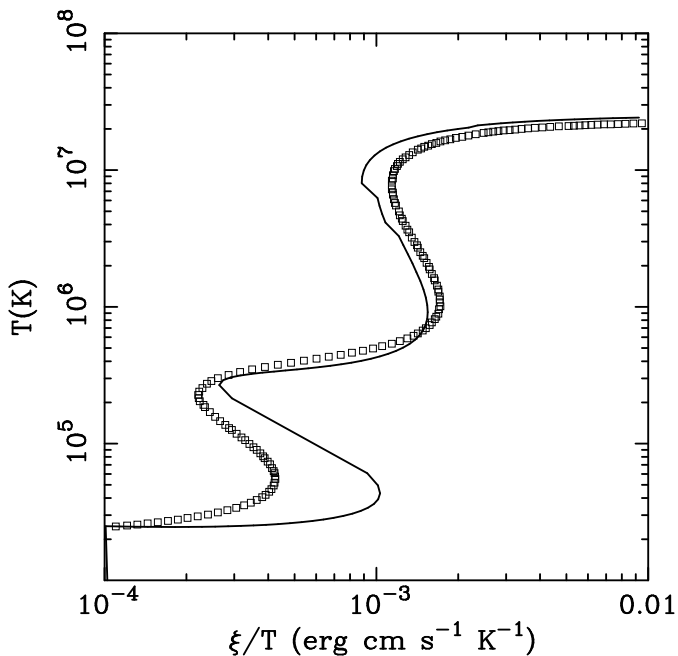


**Figure 2.** Comparison of the model (solid curve) with CLOUDY (dashed line) of a pure hydrogen/oxygen plasma.

where  $t_{sh}$  is the shortest relevant timescale<sup>§</sup>. In the case of a constant ionizing luminosity, it is found that the system always evolves to an equilibrium state, as expected.

The model has been compared against the photoionization code CLOUDY (Ferland 1996) (version 9004, (Ferland et al. 1998)) in the case of a plasma in photoionization equilibrium. Figures 2 and 3 report this comparison. There is a qualitative agreement between the model (solid line) and CLOUDY (dashed line) in figure 2 for the case of a pure hydrogen/oxygen plasma. The main goal of this paper is to reproduce the time variability of the oxygen edges, and, this figure shows how our model mirrors quite well the behavior of this element. CLOUDY includes many more physical processes and realistic elemental abundances and, as seen in figure 3, the agreement is not so good when more elements are considered<sup>¶</sup>. We have also investigated the reaction of a constant density plasma to an inverted top hat function for the light-curve (i.e. initially  $T = 10^5$  K, equal ionization fractions in each state, the luminosity is  $L = 3 \times 10^{43}$  erg s<sup>-1</sup> and held constant. The system is allowed to achieve an equilibrium at an ionization parameter  $\xi = \frac{L}{nR^2} = 75$  erg cm s<sup>-1</sup>, where  $n$  is the density of the warm plasma and  $R$  is the distance of the slab of the plasma from the

<sup>§</sup> At each step the ionization, collisional and recombination timescales of each oxygen ionization state is calculated. The shortest of these timescales is taken to be  $t_{sh}$ .

<sup>¶</sup> Realistic elemental abundances can be important both for the ionization structure and for the heating/cooling rate of the plasma, and since features of the stability curve result from peaks in the heating and cooling functions (which are in turn associated with particular ionic species), the comparison presented in figure 2 is expected to present a much better agreement. The consideration of realistic abundances is beyond the scope of this paper and is currently being studied.

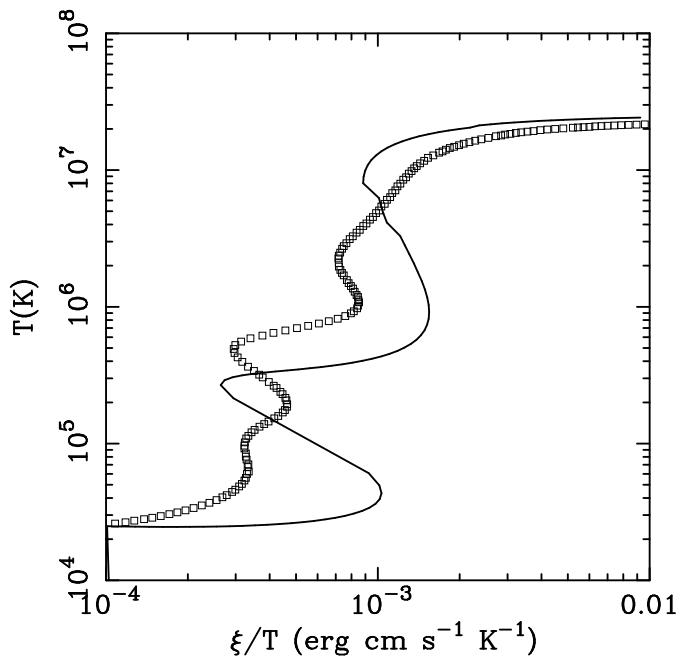


**Figure 3.** Comparison of the model (solid curve) with CLOUDY (dashed line).

ionizing source of radiation with isotropic ionizing luminosity  $L$ . The luminosity is then halved for a short period,  $\Delta t$ , and then back to its initial value). During these changes, the state of the plasma is recorded as a function of time. This choice of  $\xi$  places the inner warm absorber a region where  $f_{O8} \propto L^{-1}$  (i.e. in this regime  $f_{O8}$  is expected to be inversely proportional to  $\xi$  or equivalently to  $L$ ). The investigation has been carried out for different values of  $n$  and  $R$  keeping  $n > 2 \times 10^7$  cm<sup>-3</sup> and  $R < 1.4 \times 10^{17}$  cm (i.e. the constraints given by Otani et al. (1996) for the inner warm absorber). Fig. 4 shows an example of the results obtained. As expected,  $f_{O8}$  increases when  $L$  is halved, showing a more noticeable increment when  $L$  is halved over a longer period.

### 3 APPLICATION TO THE MCG–6-30-15 WARM ABSORBER

To reproduce the observational data using our model, it is required to obtain the value of the optical depth for OVIII once the ionization fraction  $f_{O8}$  has been calculated by the code. Considering the cross section for OVIII,  $\sigma_8$ , as constant along the line-of-sight and using the fact that the material contains only ions of oxygen in an otherwise completely ionized plasma, the optical depth for OVIII,  $\tau(OVIII)$ , can be written as:

$$\tau(OVIII) = \frac{\sigma_8 f_{O8} \Delta R n_e}{\frac{1}{Abun} + \sum_{i=1}^9 f_{O_i} \times (i-1)} \quad (6)$$

where  $\sigma_8 = 10^{-19}$  cm<sup>2</sup> (Osterbrock 1989),  $\Delta R$  is the line-of-sight distance through the ionized plasma,  $n_e$  is the electron density,  $Abun$  is the oxygen abundance relative to hydrogen (Grevesse 1989) and  $f_{O_i}$  is the ionization fraction for  $i$  ionization species for oxygen.

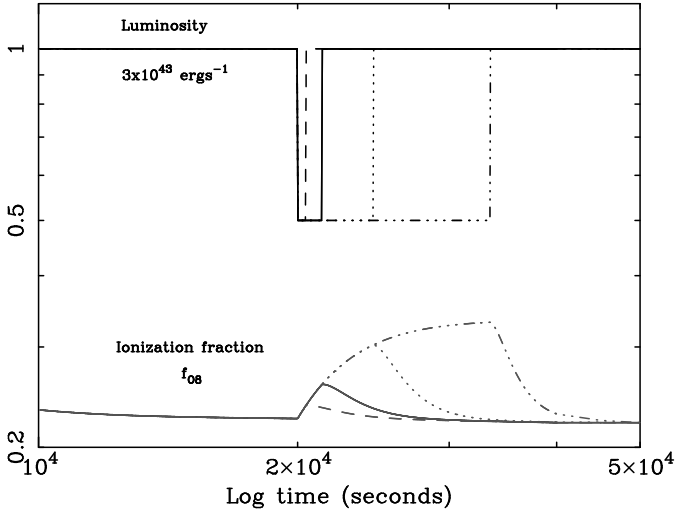


**Figure 4.** Time behaviour of the ionization fraction for OVIII,  $f_{O8}$ , for different light-curves. The plasma has ionization parameter  $\xi = 75 \text{ erg cm s}^{-1}$  for luminosity  $L = 3 \times 10^{43} \text{ erg s}^{-1}$ , electron density  $n_e = 3 \times 10^7 \text{ cm}^{-3}$  and it is situated at  $1.15 \times 10^{17} \text{ cm}$  from the ionizing source. The luminosity  $L$  is halved over an interval  $\Delta t$  equal to: 450(dashed line), 1350(solid line), 4500(dot line) and 13500(dot-dot-dot-dashed line) seconds. The corresponding ionization fraction,  $f_{O8}$ , is plotted below.

The light-curve used to reproduce the *ASCA* observation is given by Otani et al. (1996). For the *BeppoSAX* observation, the light-curve has been defined as a step function with a constant value for the luminosity  $L$  over the different time periods given by Orr et al. (1997). The constant value for  $L$  over each period is chosen to be that given in Orr et al. (1997, Fig. 3) plus a period of  $2 \times 10^4 \text{ s}$  previous to epoch 1 with  $L = 1.8 \times 10^{43} \text{ erg s}^{-1}$  (a standard value for the luminosity during the observation). Different parameters for the warm absorber have been investigated using the constraints given by Otani et al. (1996). With the only exception of point 1 (see figure 1), a general good agreement for all other experimental points is found.

Following a suggestion by Orr et al. (1997), we have modified the light-curve for the *BeppoSAX* observation including a previous epoch to it for which the luminosity is much lower (the range of values used is  $10^{40} - 10^{43} \text{ erg s}^{-1}$ )<sup>||</sup>. The reason for using this very low value for the luminosity is that in a regime for which  $f_{O8} \propto L^{-1}$ , the highest values  $f_{O8}$  are expected for low values of  $L$ . However, the suggested explanation does not reproduce the high value of  $\tau(OVIII)$  for epoch 1 in the *BeppoSAX* observation. Even for those values of  $\xi$  that give a maximum for  $f_{O8}$  (i.e.  $\xi \approx 50 \text{ erg cm s}^{-1}$ ), the ionization fraction for O(VIII) is still too low to account for the high  $\tau(OVIII)$  value at epoch 1.

<sup>||</sup> An example of a Seyfert 1 galaxy exhibiting an unusual low flux state (a decrease of more than one order of magnitude in luminosity) is presented in Uttley et al. (1999).

#### 4 A THIRD WARM ABSORBER COMPONENT

The model we propose to explain both *ASCA* and *BeppoSAX* observations incorporates a new zone for the warm absorber. Let warm absorber 1  $\equiv$  WA1 be the inner warm absorber which parameters are:  $R < 1.4 \times 10^{17} \text{ cm}$ ,  $n > 2 \times 10^7 \text{ cm}^{-3}$  and  $\Delta R \simeq 10^{14} \text{ cm}$ . The outer warm absorber will be warm absorber 2  $\equiv$  WA2 with parameters  $R > 3 \times 10^{18} \text{ cm}$ ,  $n < 2 \times 10^5 \text{ cm}^{-3}$  and  $\Delta R \simeq 10^{14} \text{ cm}$ . In our model a warm absorber 3  $\equiv$  WA3 is situated between WA1 and WA2. The WA3 radius and density will have values between those of WA1 and WA2. Therefore, while WA1 and WA2 respond on timescales of hours and weeks respectively, WA3 is expected to respond to variations in the ionizing flux on timescales of days. WA3 would have an ionization parameter  $\xi$  of the order of  $500 \text{ erg cm s}^{-1}$  for  $L = 3 \times 10^{43} \text{ erg s}^{-1}$ . Hence the ionization fraction for this value of  $L$  is too low to be detected. Only when the luminosity of the source is sufficiently low (i.e.  $\xi \approx 50 \text{ erg cm s}^{-1}$ ), WA3 reveals its presence by contributing to the total optical depth for OVIII. The medium between WA1 and WA2 would be constituted by a continuum of warm absorbers: clouds with different densities situated at different radii. Only some of them happen to be at the radius and have densities that efficiently absorbs the OVIII edge energy (i.e. most of them are undetectable). In Baldwin et al. (1995) a model for the BLR is presented, in which individual BLR clouds can be thought of as machines for reprocessing radiation. As long as there are enough clouds at the correct radius and with the correct gas density to efficiently form a given line, the line will be formed with a relative strength which turns out to be very similar to the one observed. Similarly in our model, only WA1 and WA2 are detectable for the ordinary values of the ionizing flux. Only for the case of a state of low luminosity, WA3 will be unmasked. Other zones, as yet unseen, may be present.

Assuming then the presence of WA3 and also an epoch of low luminosity previous to the *BeppoSAX* observation, the expected WA3 behaviour would be:

i) when  $L \approx 0.4 \times 10^{43} \text{ erg s}^{-1}$  (previous to epoch 1), the ionization parameter  $\xi \approx 50 \text{ erg cm s}^{-1}$ , giving a high value for  $f_{O8}$ . This period lasts for approximately  $10^5 \text{ s}$ , so the plasma has time to recombine.

ii) when  $L \approx (1, 5) \times 10^{43} \text{ erg s}^{-1}$  (i.e. during the observation), then  $\xi \approx 150, 750 \text{ erg cm s}^{-1}$ . For these high values of  $\xi$ , oxygen is practically fully stripped and therefore there is a very small contribution to the optical depth for OVIII.

The range of parameters investigated for WA3 is  $R = (2, 8) \times 10^{17} \text{ cm}$ ,  $n = 5 \times 10^5, 10^7 \text{ cm}^{-3}$  and  $\Delta R$  in the interval that gives a column density for WA3 approximately equal to  $3 \times 10^{22} \text{ cm}^{-3}$ . After taking into account the soft X-ray absorption due to WA1, the response of WA3 has been calculated and an example of the results obtained is presented in figures 5 and 6, where the general good agreement is also extended to point 1.

WA3 has also been modelled using *CLOUDY* and we found a drop in the transmitted portion of the incident continuum at  $\approx 7.8 \text{ keV}$ , of approximately 1% (i.e. undetectable for current instruments). The coronal lines strength

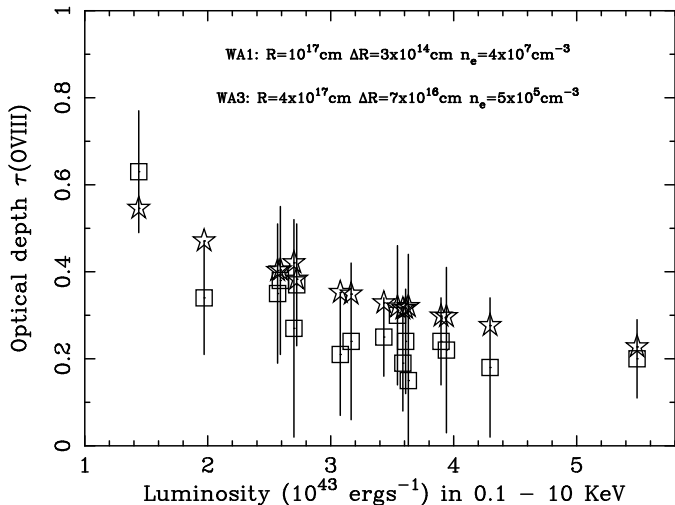


**Figure 5.** Comparison *ASCA* data (square) with the model computations (star) for the following warm absorber parameters: WA1: distance to the ionizing source,  $R = 1.0 \times 10^{17}$  cm, line-of-sight distance through the warm absorber,  $\Delta R = 3.0 \times 10^{14}$  cm, and electron density  $n_e = 4.0 \times 10^7$  cm $^{-3}$ . WA3:  $R = 4.0 \times 10^{17}$  cm,  $\Delta R = 7.0 \times 10^{16}$  cm, and  $n_e = 5.0 \times 10^5$  cm $^{-3}$ .

has also been checked using *CLOUDY*\*\* . The ratio of the modelled to observed fluxes for WA3 are all below  $0.1 \times f_c$ , where  $f_c$  is the covering fraction $^{\dagger\dagger}$ .

Finally, the contribution to  $\tau(\text{OVII})$  from each component for our model has been calculated and, as expected, we found that WA2 is the main responsible for the OVII edge (its contribution makes 96% of the total value of  $\tau(\text{OVII})$ ).

## 5 DISCUSSION

Warm absorbers have been the subject of extensive studies during the last decade. Such regions are not spatially resolved, and all the available information about their geometry is obtained from analysis of the variability of the oxygen edges. The explanation we offer for the time variability of the MCG–6-30-15 warm absorber during both *ASCA* and *BeppoSAX* observations does not invoke complex processes, but a very simple photoionization model together with the presence of a multi-zone warm absorber. This would be constituted by a continuum of clouds at different radii and different densities, such that only some of them contribute to the total optical depth for OVIII depending on the value of the luminosity.

As a final remark note how in our model WA3 is much more volume filling than WA1 ( $\Delta R/R \geq 0.1$  for WA3 while  $\Delta R/R \leq 10^{-3}$  for WA1). This suggests that WA3 could be part of the inter-cloud medium of WA1.

\*\* See Sect. 3.3 (Ferguson et al.1997) for a discussion of the state of the coronal lines atomic data used in *CLOUDY*.

$^{\dagger\dagger}$  Porquet et al. (1999) give some restrictions on the density of the WA in order to avoid producing coronal line equivalent widths larger than observed. Although WA3 presents no problems at all for any  $f_c$ , WA2 does, unless a low value of  $f_c$  is considered. This possibility is currently being investigated.

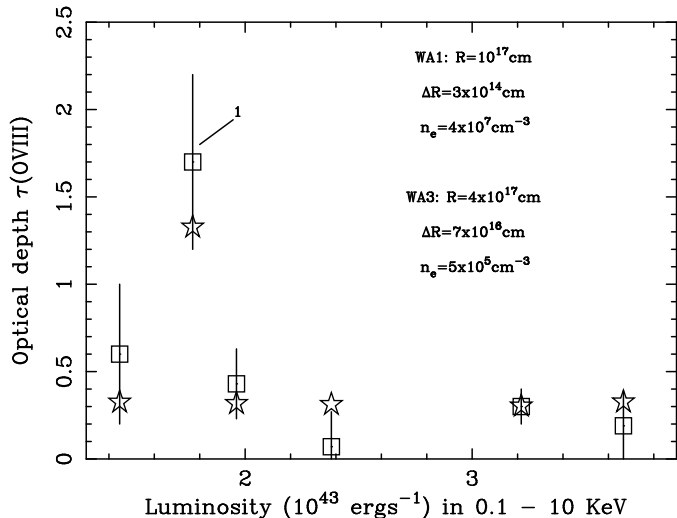


**Figure 6.** Comparison *BeppoSAX* data (square) with the model computations (star) for the following warm absorber parameters: WA1: distance to the ionizing source,  $R = 1.0 \times 10^{17}$  cm, line-of-sight distance through the warm absorber,  $\Delta R = 3.0 \times 10^{14}$  cm, and electron density  $n_e = 4.0 \times 10^7$  cm $^{-3}$ . WA3:  $R = 4.0 \times 10^{17}$  cm,  $\Delta R = 7.0 \times 10^{16}$  cm, and  $n_e = 5.0 \times 10^5$  cm $^{-3}$ .

## 6 ACKNOWLEDGMENTS

This work has been supported by PPARC and Trinity College (R.M.) and by the Royal Society (A.C.F.). C.S.R. thanks support from Hubble Fellowship grant HF-01113.01-98A. This grant was awarded by the Space Telescope Institute, which is operated by the Association of Universities for Research in Astronomy, Inc., for NASA under contract NAS 5-26555. C.S.R. also thanks support from NASA under LTSA grant NAG5-6337.

## REFERENCES

- Baldwin J., Ferland G., Korista K., Verner D., 1995, *ApJ*, 455, L119
- Fabian A. C. et al., 1994, *PASJ*, 46, L59
- Ferguson J.W., Korista K.T., Baldwin J.A., Ferland G.J., 1997, *ApJ*, 487, 122
- Ferland G.F., 1996, Hazy, a Brief Introduction To Cloudy. U. of Kentucky, Dept. of Physics and Astronomy Internal Report
- Ferland G.J., Korista K.T., Verner D.A., Ferguson J.W., Kingdon J.B., Verner E.M., 1998, *PASP*, 110, 761
- Grevesse E., N. & Anders, 1989, in Waddington C.J., ed, *Cosmic Abundances of Matter*, AIP Conference Proceedings 183. AIP, New York
- Halpern J.P., 1984, *ApJ*, 281, 90
- Orr A., Molendi S., Fiore F., Grandi P., Parmar A.N., Owens A., 1997, *A&A*, 324, L77
- Osterbrock D., 1989, Kelly A., ed, *Astrophysics of Gaseous Nebulae and Active Galactic Nuclei*. Univ. Science Books, Mill Valley, Ch. 11
- Otani C. et al., 1996, *PASJ*, 48, 211
- Porquet D., Dumont A. M., Collin S., Mouchet M., 1999, *A&A*, 341, 58
- Reynolds C. S., 1996, Ph.D. thesis, University of Cambridge
- Reynolds C. S., 1997, *MNRAS*, 286, 513
- Uttley P., McHardy I. M., Papadakis I. E., Guainazzi M., Fruscione A., 1999, *MNRAS*, accepted (astro-ph/9905104)